In-situ shelling via selective laser melting: modelling and microstructural characterisation

Qiu, Chunlei; Adkins, Nicholas; Hassanin, Hany; Attallah, Moataz; Essa, Khamis

DOI:
10.1016/j.matdes.2015.08.091

Document Version
Peer reviewed version

Citation for published version (Harvard):
Qiu, C, Adkins, N, Hassanin, H, Attallah, M & Essa, K 2015, 'In-situ shelling via selective laser melting: modelling and microstructural characterisation', *Materials & Design*, vol. 87, pp. 845-853.
https://doi.org/10.1016/j.matdes.2015.08.091

In-situ shelling via selective laser melting: modelling and microstructural characterisation

Chunlei Qiu[1*], Nicholas J. E. Adkins[1], Hany Hassanin[2], Moataz M. Attallah[1*], Khamis Essa[2*]

1: School of Metallurgy and Materials, University of Birmingham, Edgbaston, Birmingham, B15 2TT, UK
2: School of Mechanical Engineering, University of Birmingham, Edgbaston, Birmingham, B15 2TT, UK

Abstract

This study focuses on the use of selective laser melting (SLM) to produce tooling (a shell) that is filled with powder and subsequently consolidated via hot isostatic pressing (HIPing) so that the tooling, rather than being removed, becomes part of the sample. The microstructures of HIPed samples were studied using scanning electron microscopy (SEM) and electron backscattered diffraction (EBSD) to assess the bond between the shell and the consolidated powders. The columnar grains in the SLM-built tooling bonded with the powder although the grains in the tooling were found to be much coarser than those in the HIPed powder, leading to preferential failure in the tooling. However, failure occurred in a fairly ductile mode and reasonable tensile strengths and ductility were obtained. Finite element models were developed to define the required initial shape of the shell in order to obtain the correct geometry after HIPing. It was found that the final shapes predicted are consistent with the observations on HIPed samples.

Key words: Selective laser melting; in-situ shelling; modelling; hot isostatic pressing; microstructure; tensile behaviour

[*]Corresponding authors: Tel: (+44) 121 414 7842; fax: (+44) 121 414 7890;

E-mail addresses: c.qiu@bham.ac.uk (C.L. Qiu), m.m.attallah@bham.ac.uk (M.M. Attallah), K.E.A.Essa@bham.ac.uk (K.E.A. Essa).

1. Introduction

Additive manufacturing such as selective laser melting (SLM) and near-net-shape hot isostatic pressing (HIPing) are effective near-net-shape manufacturing technologies. Particularly, SLM has the capacity to fabricate complex freeform geometries directly from computer-aided design (CAD) models. One disadvantage of SLM process is that their building rate is usually low due to the processing limit on powder layer thickness [1-3]. As a result, it is time-consuming to build large parts especially when the parts contain large cross sections or thick walls. Net-shape HIPing, by contrast, could be more efficient in processing rate. However, it involves the design and preparation of capsules for powder filling as well as modelling to predict shape change during HIPing. The capsules or tooling are usually made of steels and need to be removed after HIPing either by pickling or machining which is expensive [3].

In the present work, we use a hybrid route, in-situ shelling route which combines the strengths of SLM and HIPing, which was initially suggested by Das et al [5], more than a decade ago. The idea is to use SLM to prepare thin tooling with specific shapes which are then filled with powder and HIPed to required shapes. In Das et al's work [5], the focus was on microstructural development of the samples fabricated by SLS (selective laser sintering) plus HIPing. No report on the tooling design, shape change during HIPing as well as as-fabricated components was made. In this study, we use modelling to predict the shape change of the tooling during HIPing, which in turn creates feedback to the design of the tooling. Modelling on hot isostatic pressing has made significant advance in the past two decades. Shima and Oyane [6] proposed a plasticity theory for porous metals, which represents the basis for most of the powder consolidation modelling work. Cassenti [7] investigated HIPing modelling using an elasto-plastic large-deformation model with implicit thermal calculations.

Later, Nohara et al. [8] and Abouaf et al. [9-13] developed and adapted constitutive equations to account for elasticity, visco-plasticity, and thermal effects, and to model the mechanical behaviour of the powder. Similar finite element (FE) models were also developed by Svoboda et al. [14-16], and Wikman et al. [17] who developed a combined material model that accounts for both granular and viscoplastic behaviours whereby the granular plasticity model accounts for the early stage of the consolidation and the viscoplastic model accounts for the intermediate and later stages of consolidation. Gillia et al. [18] further improved the viscoplastic model by taking into account the strain hardening effect of the powder material. Samarov et al. [19] developed a FE model to predict the final dimensions of shaped part produced by HIPing Ti-6Al-4V powder, using the constitutive equations for plastic yielding, without considering the constitutive models that describe other densification mechanisms. This was justified because more than 90% of density increase occurs within this instantaneous plastic yield mechanism. This model has relative concise formulation with fewer parameters involved as reported by Seliverstov et al. [20]. The developed model showed very good agreement of more than 98% between the produced geometries and the predicted ones. Similar conclusion was reported by Wei et al [21] who suggested that the creep mechanism does not play a major role in the powder consolidation during HIPing, for instance at the ramp up and cooling down parts of the HIP cycle. Khoei et al [22] employed a constitutive model based on the double-surface plasticity to simulate the thermo-mechanical compaction process and to predict the relative density, temperature and stress distributions. However, the ability of the model to predict the shrinkage shape change was not presented.

Recently, constitutive models that account for densification mechanism by plasticity and creep were used to improve the prediction accuracy of HIP macroscopic models. Aryanpour et al [23] used plastic–viscoplastic model to simulate the powder densification in HIPing. The results were validated against published 316LN stainless steel data and good agreement was

found. However, the model prediction was only limited to the relative density. Similar model was used by Liu et al [24] who investigated the influence of pressure on the densification behaviour of 316L stainless steel powder using a modified PERZYNA model. The model used to predict the shape change of a 2D cylinder with a relative error of about 7%. Though, these approaches are complex and need large computation time compare with pure plasticity models [19, 22].

In this paper, several simple shapes including cylindrical and annular samples have been selected to try the in-situ shelling route. FE modelling is developed to predict the final shape of the tooling after HIPing, which is integrated to the design of initial shape of tooling. The microstructure and tensile behaviour of the SLMed+HIPed samples are also evaluated.

2. Modelling and Experimental

2.1 Constitutive equations

In this investigation, a material model based on the modified Gurson's porous metal plasticity theory has been used. This material model defines the inelastic flow of the porous metal on the basis of a potential function that characterises the porosity in terms of relative density as shown in Equation (1).

$$\phi(\sigma,\rho)=\left(\frac{q}{\sigma_y}\right)^2+2q_1(1-\rho)Cosh\left(-q_2\frac{3P}{2\sigma_y}\right)-1(q_3(1-\rho))^2=0 \quad (1)$$

$$q=\sqrt{\frac{3}{2}\mathrm{S}:\mathrm{S}} \quad (2)$$

$$P=-\frac{1}{3}\sigma:\mathrm{I} \quad (3)$$

Where q is the effective Mises stress, σ_y is the yield strength of a material, S is the deviatoric part of the Cauchy stress tensor σ, P is the hydrostatic pressure, ρ is the relative density and q_1, q_2 and q_3 are material parameters and were introduced by Tvergaard [25]. When $q_1 = q_2 = q_3 = 1$, Equation (1) reduces to the yield function originally proposed by Gurson's [26].When $q_1 = q_2 = q_3 = 0$, Equation (1) reduces to the usual Mises stress.

The relation for the dependence of the elastic modulus on the relative density is shown in Equation (4) as proposed by Gillia et al [18] where they modified the model obtained from cold compacted samples. A similar model was also developed by Svoboda et al. [14-16]. Equation (5) establishes the dependence of the thermal conductivity upon relative density as proposed by Argento and Bouvard [27] which is relevant either at low density or at high density.

$$E(\rho, T) = E(1, T)(0.1 + 0.9\rho^{12}) \tag{4}$$

$$K_{eff} = K_s \left(\frac{\rho - \rho_o}{1 - \rho_o} \right)^{\frac{3}{2}(1-\rho_o)} \tag{5}$$

Where $E(1,T)$ is the modulus of elasticity of the solid at temperature (T), K_{eff} is the effective thermal conductivity, K_S is the thermal conductivity of the solid ρ_o is the initial relative density. The powder is modelled using the modified Gurson's porous metal plasticity theory while the mild steel container is modelled using the conventional Mises deformation equations. The material model described above is implemented in the implicit coupled temperature-displacement solver of the ABAQUS software. The thermo-elastic models, Equation 4-5, are implemented into user-defined model.

In this study, we aimed at fabricating two axis-symmetric demonstrators, a cylinder and a hollow cylinder (annular), using the proposed in-situ shelling route through both 2D

modelling and experimental trials. The required dimensions of these samples are shown in Fig. 1(a) and Fig. 2(a), respectively. The whole design and manufacturing process involves initial prediction of the powder response and shape changes (FEM model), subsequent tooling design and SLM fabrication of tooling and final realisation of the target shape through HIPing. As a start, an initial guess of the tooling is designed which will then go through FE modelling. The final shape is predicted by the modelling and compared with specified shape. If the required dimensions are not achieved a new iteration will be performed until the modelling agrees with observation within an acceptable error. Fig. 1(b-c) and Fig. 2(b) show the initial tooling design for two models and their corresponding final shapes predicted by modelling are shown in Fig. 1(d-e) and Fig. 2(c), respectively. To simplify things, the angles at the corners have been made right angles and the internal surfaces of the tooling have all been made straight along height direction and only the outer surfaces made curved. Both the basic wall thickness (t, as shown in Fig. 1 and 2) and curvature (radius) of the outer surfaces have been changed for tooling design so that specified shapes could be achieved in the modelling for HIPing. In reality, because the top needs to be connected with a filling tube (see Fig. 3), both the internal and outer surfaces of the top wall were made at a slant angle and as a result there would be a powder reservoir on the top. The top wall thus would not fit with the modelling both before and after HIPing.

In the models, the powder is partitioned within the container geometry to provide a rigid contact between the powder and the inner surfaces of the container. The powder geometry is meshed with 8-node quadrilateral elements and the container geometry is meshed with elements from the same type. Coarser mesh size was found to lead to less accurate prediction of the relative density. The solution has converged at 0.5mm element size. Boundary conditions are the following: the pressure load is applied to all free edges of elements and the temperature is prescribed for the nodes along theses edges. The heating rate is 5 °C/min up to

920 °C with a dwell time of 4 hours. The cooling rate is 5 °C/min. Pressure profile is similar in time and goes up to 100 MPa. Axisymmetric displacement boundary condition is applied in the X-direction along the centre line.

Two different types of material description are assumed in the computational model. Material model for the Ti-6Al-4V tooling is assumed thermal-elastoplastic with temperature-dependent mechanical and thermal properties. The powder material is modelled using data for Ti-6Al-4V. The thermal properties with temperature dependence are found in [28]. Flow curves for the compacted powder at different temperature and different strain rates are used [28].

2.2 Materials and experimental procedure

Gas atomised Ti-6Al-4V powder supplied by TLS Technik GmbH in the size range of 25~50 µm was used. A Concept Laser M2 Cusing SLM system which employs an Nd:YAG laser with a wavelength of 1075 nm and a constant beam spot size of 50 µm in diameter and a maximum laser output power of 400 W and a maximum laser scanning speed of 4000 mm/s has been used to prepare in-situ powder filled cans for characterisation, HIPing and testing. The tooling was fabricated at a laser power of 400 W and a laser scanning speed of 2400 mm/s using an island scanning strategy which has been detailed in previous work [1]. HIPing was performed at 920 °C/100 MPa/4 h. The as-fabricated samples were then sectioned along different directions and ground using grinding papers ranging from 240 grits up to 2500 grits. The samples were then firstly polished in a suspension containing diamond particles of 3µm in diameter and finally in activated colloidal silica solution prior to characterisation using optical microscopy (OM), scanning electron microscopy (SEM) and electron back scattered diffraction (EBSD) in a JEOL 7000 FEG-SEM microscope to study the microstructure and bonding between HIPed powder and SLMed+HIPed tooling. Some samples were further

etched in an etchant containing 50 ml distilled water, 25 ml HNO_3 and 5 ml HF for microstructural investigation using SEM. The SEM was generally operated under 20 KV.

Tensile tests were performed at room temperature using a computer-controlled electric screw driven Zwick/Z100 tensile testing machine on the samples that contain both HIPed powder and SLMed+HIPed tooling. Cylindrical specimens with a gauge length of 20 mm and a diameter of 4 mm within the gauge range were used for the current tensile testing. The tests were conducted under strain control mode with a strain rate of $1.0x10^{-3}$ s^{-1}. Tested specimens were examined using OM and SEM.

3. Results and Discussion

3.1 Modelling results

Fig.1-Fig. 3 show the shape change of as-SLMed tooling (cylindrical tooling and annular tooling) after HIPing through both modelling and experiment. It can be seen that the predicted final shapes are fairly consistent with observation with the maximum deviation less than 1.3 mm. It is also obvious that heterogeneous deformation occurs throughout the samples. Maximum deformation always occurs in the middle region of the tooling (including lateral and bottom walls) probably due to the lower physical constraint at those locations, i.e. reduced stiffness. Thus, the curved design for the walls of which the middle regions are thicker than the rest seems to work well in accommodating the heterogeneous deformation to develop relatively uniform and straight final walls as required. It is also noted that with decreased wall thickness (t), increased wall curvature is required to achieve specified straight final walls after HIPing. This is because decreased wall thickness means increased volume of loose powder particles within the tooling which could lead to increased shrinkage (particularly around the middle regions of the walls) during HIPing. With increased curvature, the actual wall thickness in the middle region will be increased to accommodate the

significant deformation there. For the annular tooling, more deformation actually occurs from the outer O-ring wall (see Fig. 2(d)) because of the higher force exerted on it, since the surface area of the outer O-ring is larger than that of the inner O-ring while the pressure is isostatic during HIPing. The detailed consolidation and deformation mechanisms of the tooling will be described elsewhere.

3.2 Microstructure

Fig. 4 shows a longitudinal section of an as-HIPed sample containing SLMed+HIPed tooling and HIPed powder in as-polished state. There is no visible gap or boundary between the tooling and the HIPed powder, even after etching (see Fig. 5), suggesting that a good bonding between the tooling and HIPed powder has been achieved. This is further supported by the observation on a longitudinal section along the build direction (or Z direction) where no obvious boundary between the lateral walls and the HIPed powder could be observed; see Fig. 6. However, the difference in microstructure between the tooling and HIPed powder was found to be pronounced. The tooling tends to show well developed basket-weave lamellar structure (Fig. 5d) and large columnar grains (Fig. 6d) whereas the as-HIPed powder contain much finer equiaxed grains and randomly distributed lamellar structure. Some of the columnar grains in the tooling show widths larger than 100 μm and length beyond 1 mm (Fig. 6d) whereas the grain size (diameter) of as-HIPed powder is generally below 10 μm. α laths in the tooling are also much longer than those in the as-HIPed powder. The columnar grains in Ti-6Al-4V after SLM have been well reported and are generally attributed to the directional cooling (heat sinks down towards cold substrate) during SLM [1-2]. Moreover, the as-SLMed Ti-6Al-4V could develop very long martensitic needles that can extend through a large grain or several neighbouring grains [1]. These needles would transform into long α laths after HIPing (which could act as a heat treatment), as observed in the current

study. In contrast, HIPing, with no melting involved and with isostatic heating and cooling, the equiaxed grains in gas atomised powder particles could be retained after HIPing. Although HIPing temperature may change the grain size, it will not change their morphology significantly. Also, with the randomly distributed and much finer equiaxed grains, the microstructural development such as α and β laths would be constrained within each grain and thus their lengths would be much smaller as compared with those in SLMed+HIPed samples. That the current SLMed samples contain large columnar grains is believed to be due to the use of high laser power (400W). In our previous study where low laser power (200W) was used, the grain structure was finer and the tensile strengths are much better (around 150MPa higher) [1]. The comparison suggests that the microstructure within tooling could be further optimised through selection of processing condition.

The difference in microstructure between the tooling and HIPed powder is also evidenced in EBSD analysis results, as shown in Fig. 7. The tooling shows a strong micro-texture with α laths preferentially oriented in a certain directions, particularly along $<11\bar{2}0>$ (Fig. 7e), consistent with SEM observation (Fig. 6d) where α laths always lie in slant angles. According to Thijs et al [1], the growth direction of martensitic needles is parallel to the local conductive heat transfer directions which are usually dispersive and thus could promote the formation of slanted α′ needles. Texture is also observed along <001> (Fig. 7f), obviously due to the development of columnar prior β grains which usually grow vertically or along the building direction as a result of the thermal difference between substrate and melted material. The HIPed powder, in contrast, shows almost no texture as evidenced by Fig. 7g-h, confirming that the grains in HIPed powder side are randomly oriented.

3.3 Tensile properties and fracture

Fig. 8 shows the tensile testing results for the specimens that contain SLMed+HIPed tooling and as-HIPed powder. All the specimens tested show comparable tensile properties. Investigation on the tested specimens suggests that failure does not occur at the interface between the SLMed+HIPed tooling and HIPed powder, further suggesting that a good bond has been achieved at the interface. Instead, failure was found to occur on the side of SLMed+HIPed tooling. The fracture is fairly ductile as indicated by the development of necking (Fig. 9a) in the tested specimens. Cavities were also developed near the fracture surface (Fig. 9d) characteristic of necking failure, and were not present in the area away from the fracture surface. That the failure occurred on the side of tooling is believed to be due to the much coarser microstructure (as shown above) developed within the tooling. The large columnar grains may have lower yield strength and ultimate tensile strength as compared with the HIPed powder which contain much finer equiaxed grains. As a result, plastic deformation and fracture happened first on the side of the tooling. This is further supported by the observation on the tensile tested samples (Fig. 9a) where the HIPed powder side remains fairly straight after testing (implying low and homogeneous deformation) while the tooling side shows pronounced reduction in cross section towards the fracture surface, indicative of significant deformation of the tooling.

4. Conclusions

1) The in-situ shelling route supported by modelling is feasible for producing simple axis-symmetrical components.
2) The current modelling that only considers plastic yielding was found to be effective in predicting the final shapes of the current tooling after HIPing.
3) Maximum deformation occurred in the least constrained middle region of tooling.

4) Decreased wall thickness requires higher curvature for the tooling to be deformed to required shapes.
5) Good bonding between the SLM-built tooling and the consolidated powders has been achieved after HIPing.
6) The SLMed+HIPed tooling tends to show coarse columnar grain structure and α lamellar structure whereas the HIPed powder show much finer randomly oriented grains and α laths, leading to failure on the side of tooling during tensile testing.

Acknowledgements

The work shown in this paper is part of an AMAZE project (Additive Manufacturing Aiming towards Zero Waste and Efficient Production of High-Tech Metal Products) and was financially sponsored by the Seventh European Frame Programme (FP7). Thanks are extended to Dr. Jianglin Huang for useful discussion and help in developing the current modelling, Professor Michael.H.Loretto for useful discussion and Manufacturing Technology Centre (MTC) for conducting the GoM scanning of as-HIPed samples.

References

[1] Qiu CL, Adkins NJE, Attallah MM. Microstructure and tensile properties of selectively laser-melted and of HIPped laser-melted Ti–6Al–4V. Mater Sci Eng A 2013;578:230–9.
[2] Thijs L, Verhaeghe F, Craeghs T, Van Humbeeck J, Kruth J-P. A study of the microstructural evolution during selective laser melting of Ti–6Al–4V. Acta Mater 2010;58: 3303–12
[3] Xu W, Brandt M, Sun S, Elambasseril J, Liu Q, Latham K, Xia K, Qian M, Additive manufacturing of strong and ductile Ti–6Al–4V by selective laser melting via in situ martensite decomposition. Acta Mater 2015;85: 74–84
[4] Qiu CL, Attallah MM, Wu XH, Andrews P. Influence of hot isostatic pressing temperature on microstructure and tensile properties of a nickel-based superalloy powder. Mater Sci Eng A 2013;564:176–85
[5] Das S, Wohlert M, Beaman JJ, Bourell DL. Processing of titanium net shapes by SLS/HIP. Mater Des 1999;20:115-21.
[6] Shima S, Oyane M. Plasticity theory for porous metals. Int J Mech Sci 1976;18: 285-91.
[7] Cassenti BN. The manufacture of disks by the hot isostatic pressing process. AIAA J, 1980; 80:111l.
[8] Nohara A, Nakagawa T, Soh T, Shinke T. Numerical simulation of the densification behaviour of metal powder during hot isostatic pressing. Int J Numer Meth Eng 1988; 25:213-25.
[9] Abouaf M. Modelisation de la compaction de poudres metalliques frittees. PhD Thesis, Universite Scientifique et Medical de Grenoble, 1985.
[10] Abouaf M, Chenot JL, Raisson G, Bauduin P. Finite element modeling of hot isostatic pressing process of metal powders. in Proceeding of NUMIFORM conference. 1986.
[11] Abouaf M, Chenot JL, Bauduin P, Raisson G. Prediction of the deformation during the production of near net shape superalloy parts by hot isostatic pressing process, in 2nd International Conference on Isostatic Pressing. 1982.
[12] Abouaf, M. Finite element simulation of hot isostatic pressing of metal powders. Int J Numer Meth Eng 1988; 25;191-212.
[13] Bensson J, Abouaf M. Finite element simulation of hot isostatic pressing process of ceramic powders. In 2nd International Conference on Isostatic Pressing-Theory and Applications. Gaitherburg, 1989

[14] Svoboda A, Häggblad H-ÃK, Karlsson L. Simulation of Hot Isostatic Pressing of a powder metal component with an internal core. Comput Method Appl Mech Eng. 1997;148:299-314.
[15] Svoboda A, Lindgren L-E, Oddy AS. The effective stress function algorithm for pressure-dependent plasticity applied to hot isostatic pressing. Int J Numer Meth Eng 1998;43: 587-606.
[16] Svoboda A, Nasstrom M. Simulation of hot isostatic pressing of metal powder components to near net shape. Eng Comput 1996;13: 13-37.
[17] Wikman B, Svoboda A, HÃggblad HÃ. A combined material model for numerical simulation of hot isostatic pressing. Comput Method Appl Mech Eng 2000;189:901-13.
[18] Gillia O, Boireau B, Boudot C, Cottin A, Bucci B, Vidotto F. Modelling and computer simulation for the manufacture by powder HIPping of blanket shield components for ITER. Fusion Eng Des 2007;82:2001-7.
[19] Yuan WX, Mei J, Samarov V, Seliverstov D, Wu X. Computer modelling and tooling design for near net shaped components using hot isostatic pressing. J Mater Proc Tech 2007; 182:39-49.
[20] Seliverstov D, Samarov V, Goloviskin V, Alexandrov S, Ekstrom P. Capsule design for hip of complex shape parts. In Proceedings of the International Conference on Hot Isostatic Pressing. Rotterdam, 1993.
[21] Wei QS, Xue PJ, Liu GC, Lu H, Huang J, Shi YS. Simulation and verification of near-net shaping a complex-shaped turbine disc by hot isostatic pressing process. Int J Adv Manuf Tech 2014;74: 1667–77.
[22] Khoei AR, Molaeinia Z, Keshavarz S. Modeling of hot isostatic pressing of metal powder with temperature–dependent cap plasticity model. Int J Adv Manuf Tech 2013;6: 363-76.
[23] Aryanpour G, Mashl S, Warke V. Elastoplastic–viscoplastic modelling of metal powder compaction: application to hot isostatic pressing. Powder Metall 2013;56: 14-23.
[24] Liu GC, Shi YS, Wei QS, Xue PJ. Simulation of pressure effects on hot isostatic pressing of stainless steel powder. J Central South Uni 2012;19: 55-62.
[25] Tvergaard V. Influence of voids on shear band instabilities under plane strain conditions. Int J Fract 1981;17:389-407
[26] Gurson AL. Plastic flow and fracture behaviour of ductile materials incorporating void nucleation, growth and coalescence. PhD thesis, Brown University, 1975.

[27] Argento C, Bouvard D. Modelling the effective thermal-conductivity of random packing of spheres through densification. Int J Heat Mass Transfer 1996;39:1343-50

[28] Turner RP. Linear friction welding of Ti-6Al-4V: modelling and validation. PhD thesis, the University of Birmingham, 2010

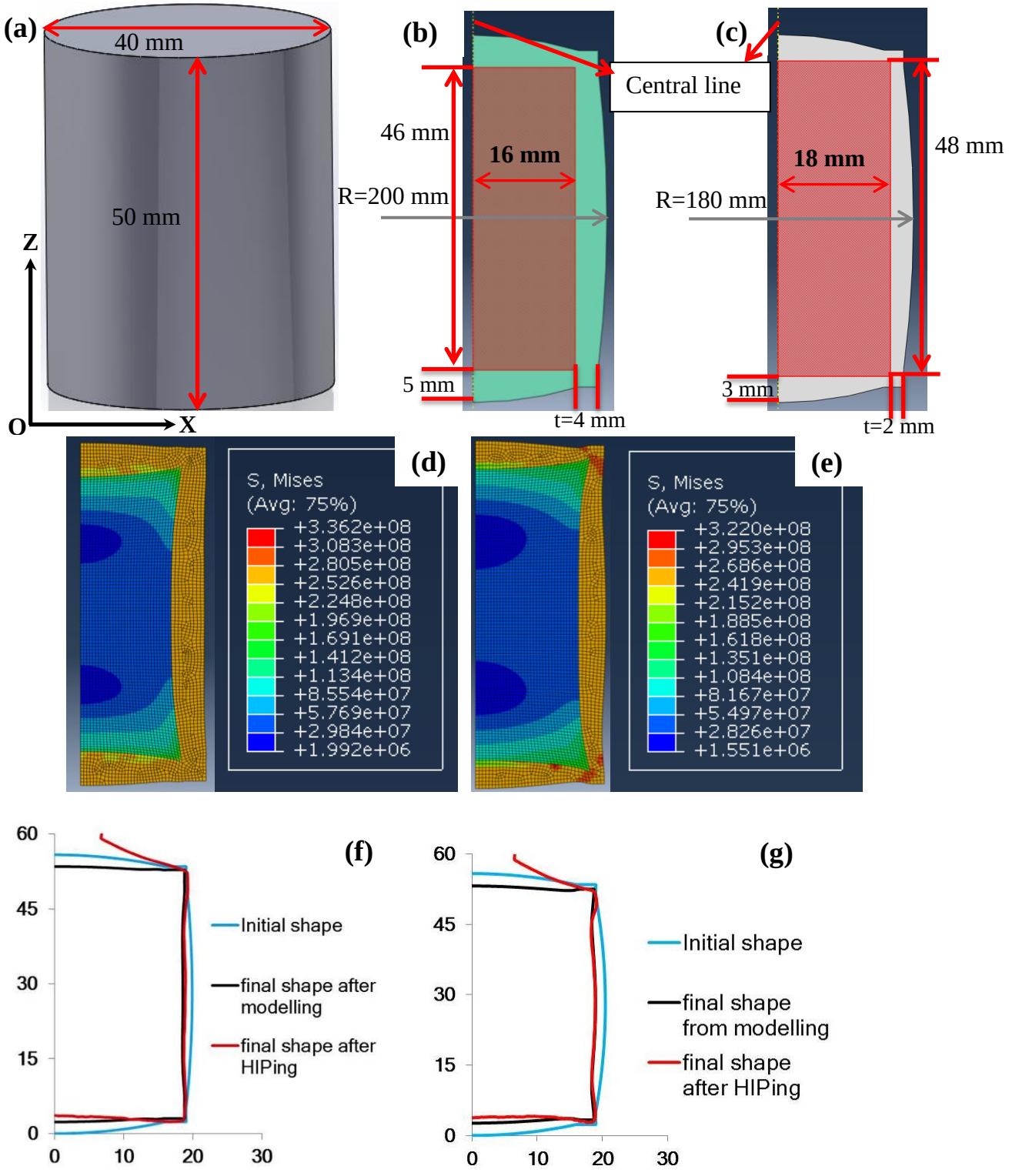

Fig. 1 (a) Specified final cylindrical sample to be fabricated via in-situ shelling route; (b) initial tooling shape with wall thickness t=4 mm; (c) initial tooling shape with t=2 mm; (d) predicted final shape after HIPing of the tooling shown in (b); (e) predicted final shape after HIPing of the tooling shown in (c); (f) shape change of the tooling with t=4 mm during

HIPing through modelling and experiments; (g) shape change of the tooling with t=2 mm during HIPing through modelling and experiments.

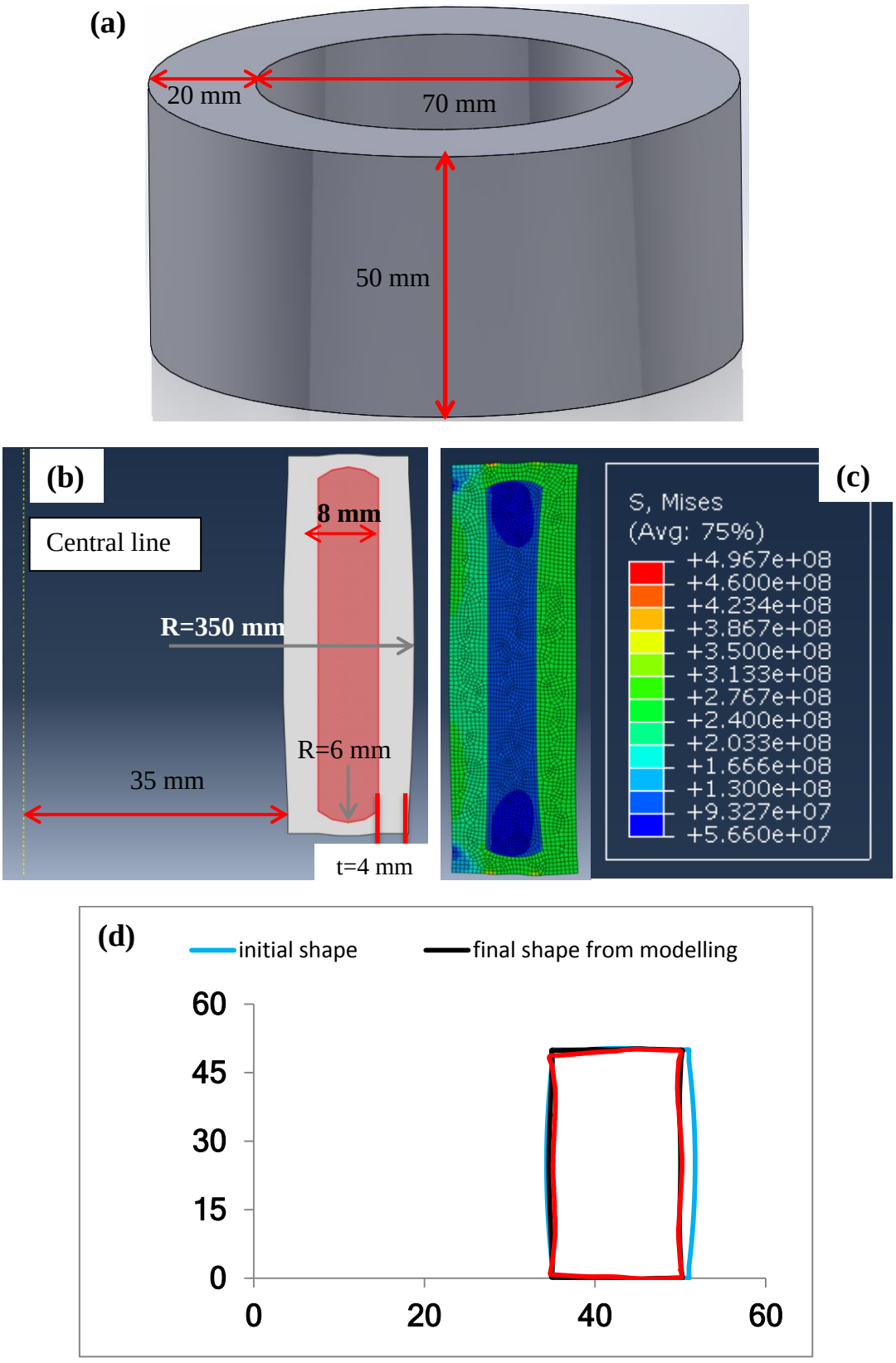

Fig. 2 (a) Specified final annular sample to be fabricated via in-situ shelling route; (b) initial tooling shape with wall thickness t=4 mm; (c) predicted final shape after HIPing the tooling shown in (b); (d) shape change before and after HIPing through modelling and experiments.

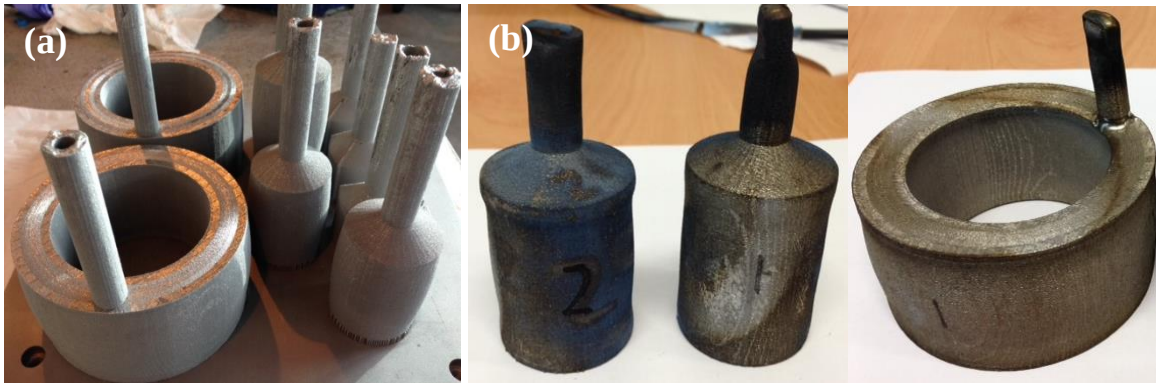

Fig. 3 Photographs showing several tooling designs (a) before and (b) after HIPing

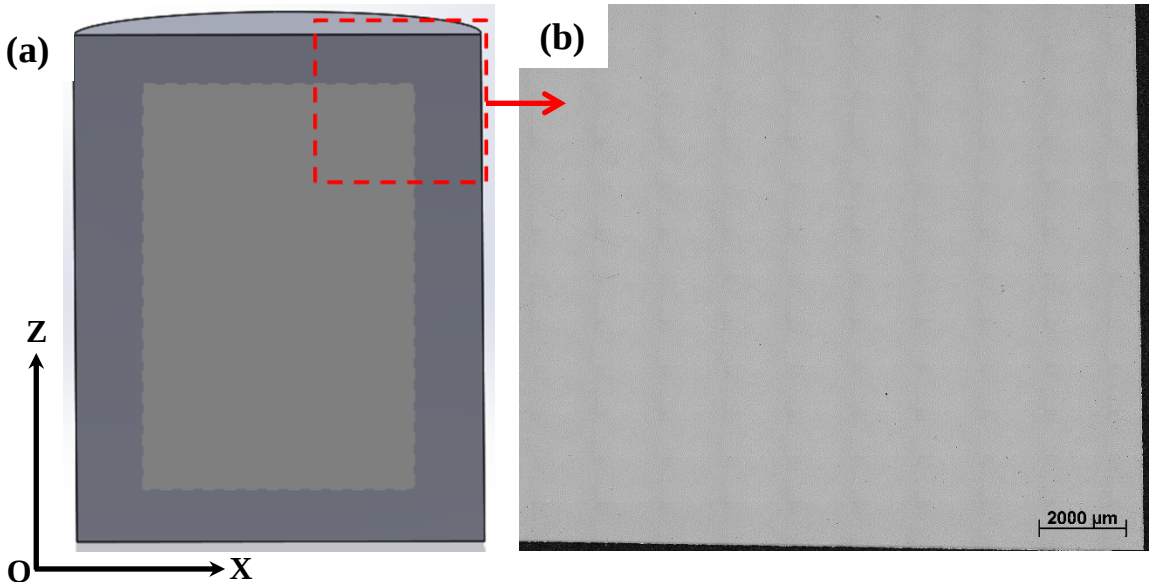

Fig. 4 (a) Schematics showing a longitudinal section that has been obtained for OM characterisation; (b) OM micrograph showing no gap or obvious boundary between a SLMed+HIPed tooling and HIPed powder after HIPing.

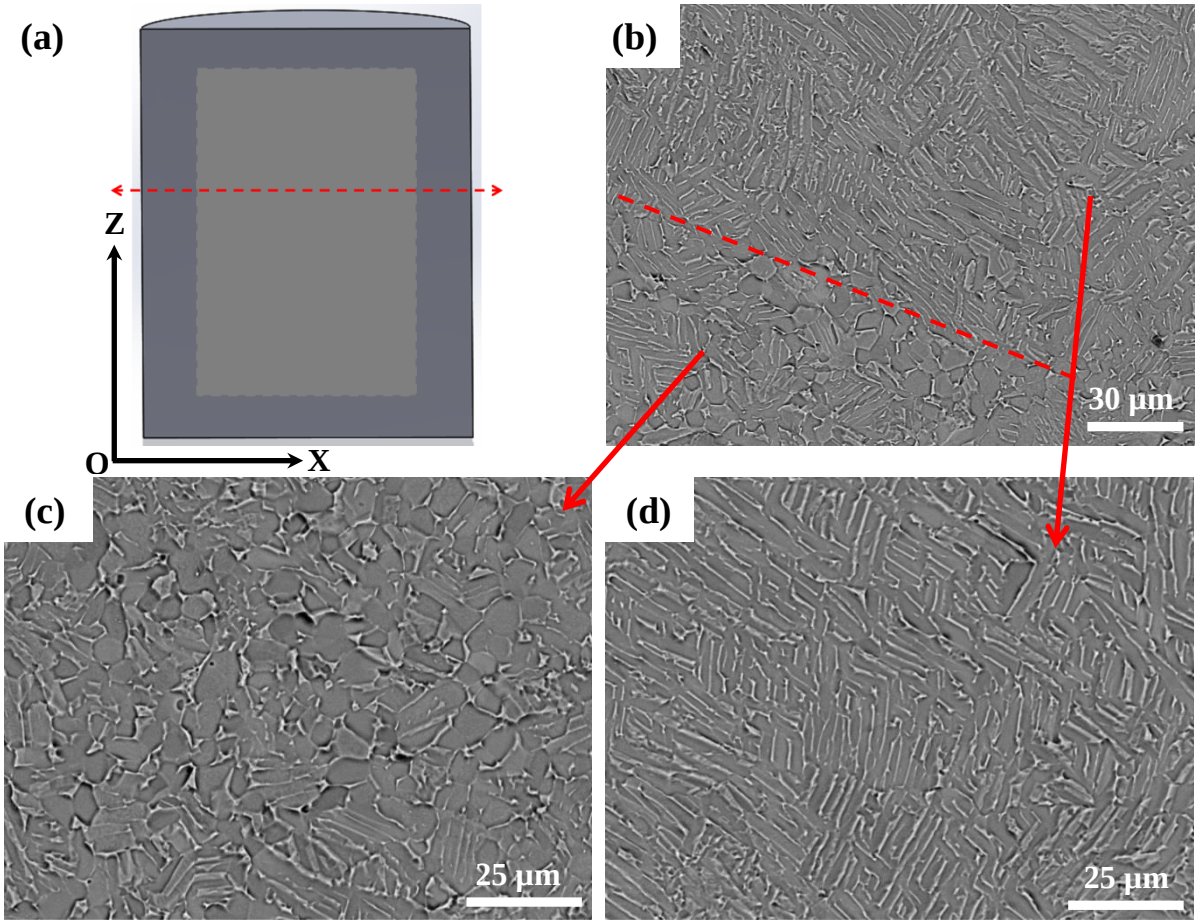

Fig. 5 (a) schematic illustration of a cross section (XY plane) for SEM characterisation, (b) microstructure at the interface between tooling and HIPed powder; (c) microstructure on the side of the tooling; (d) microstructure on the side of the HIPed powder

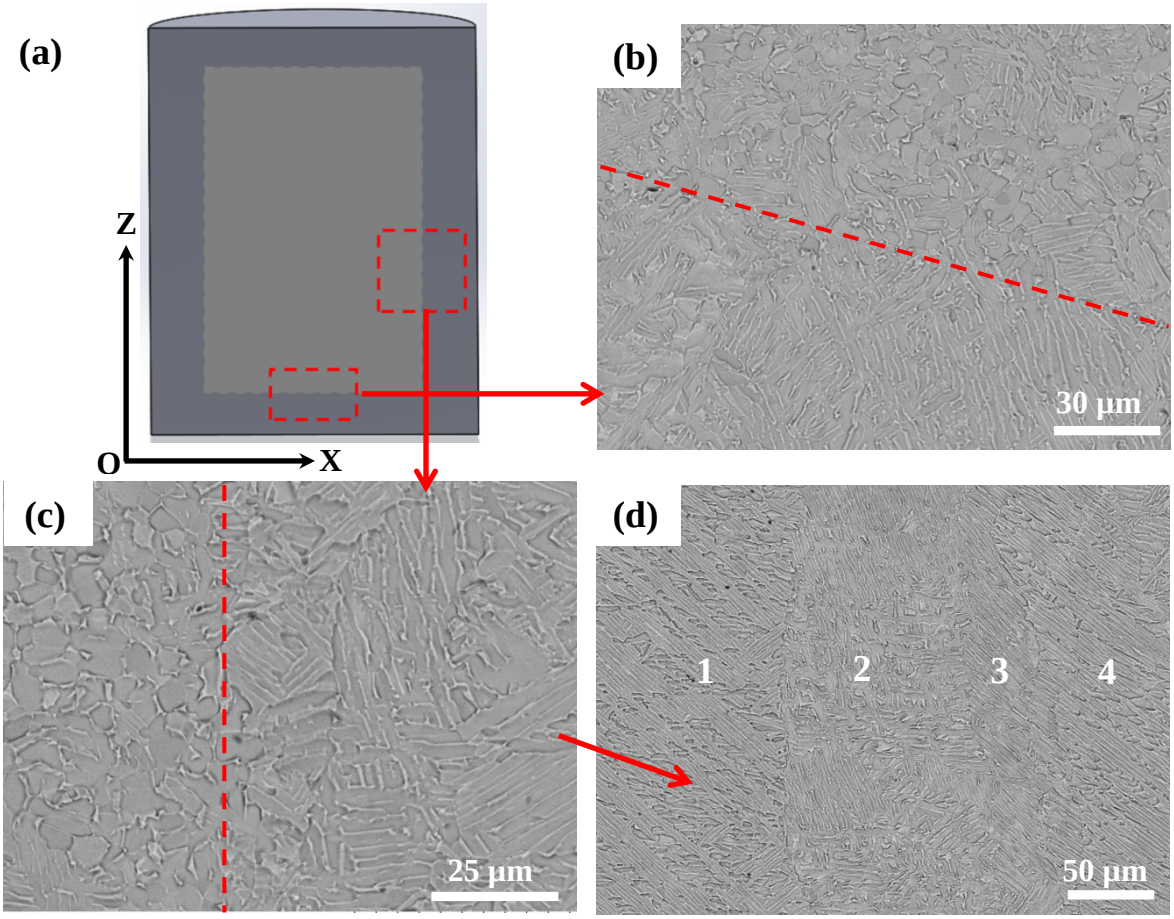

Fig. 6 (a) Schematic illustration of a vertical section (XZ plane) for SEM characterisation; (b) microstructure at the interface between the bottom wall and HIPed powder; (c) microstructure at the interface between a lateral wall and HIPed powder; (d) microstructure within the SLMed+HIPed tooling. The numbers in (d) represent several different columnar grains.

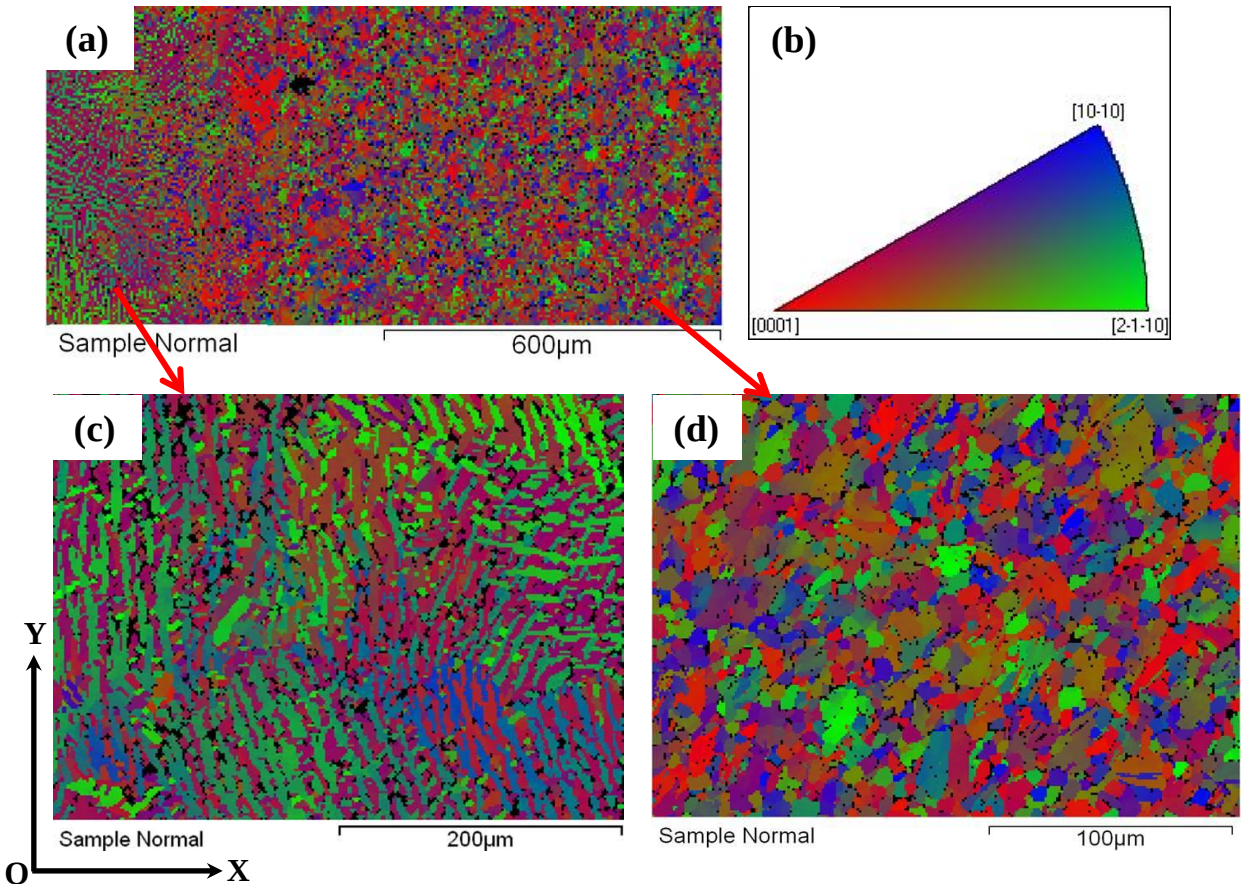
(a)
Sample Normal
600μm
(b)
[10-10]
[0001]
[2-1-10]
(c)
Sample Normal
200μm
(d)
Sample Normal
100μm
Y
O
X

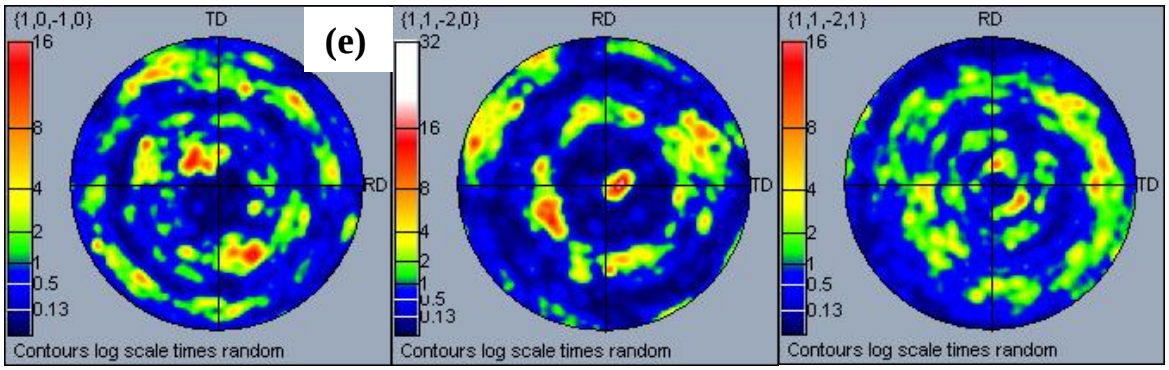
(e)
{1,0,-1,0}
TD
RD
{1,1,-2,0}
RD
TD
{1,1,-2,1}
RD
TD
16
8
4
2
1
0.5
0.13
32
Contours log scale times random

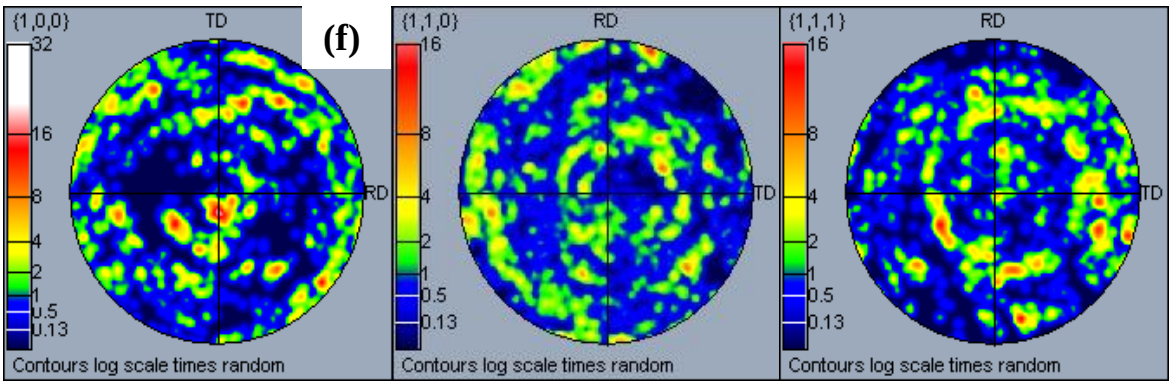
(f)
{1,0,0}
TD
RD
{1,1,0}
RD
TD
{1,1,1}
RD
TD
32
16
8
4
2
1
0.5
0.13
Contours log scale times random

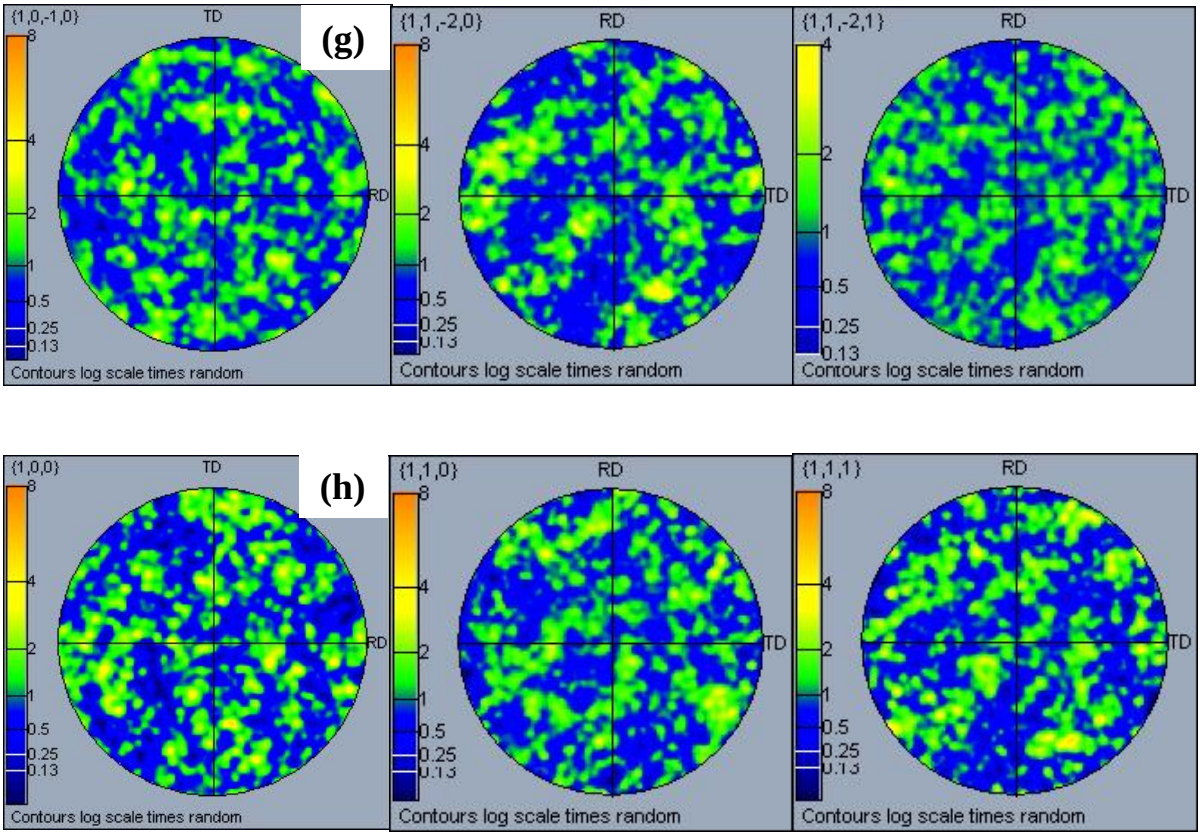

Fig. 7 EBSD micrographs showing (a) microstructure at interface between SLMed+HIPed tooling and HIPed powder; (b) inverse pole figure for (a); (c) microstructure within the tooling and (d) microstructure in as-HIPed powder; (e) α phase pole figure and (f) β phase pole figure for SLMed+HIPed tooling; (g) α phase pole figure and (h) β phase pole figure for HIPed powder.

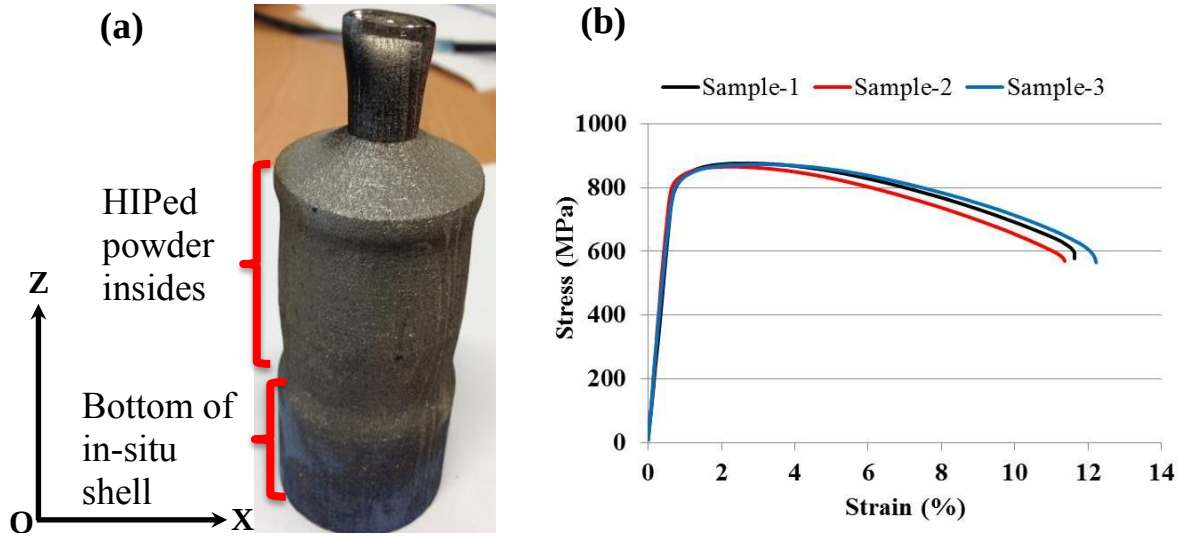

Fig. 8 (a) Photograph of the SLMed+HIPed sample from which tensile specimens were prepared; the bottom of the tooling was purposely thickened so that the machined tensile specimens would contain half material from the tooling; (b) tensile testing results for specimens containing tooling and HIPed powder after HIPing. Sample 1, 2 and 3 were all machined along Z direction.

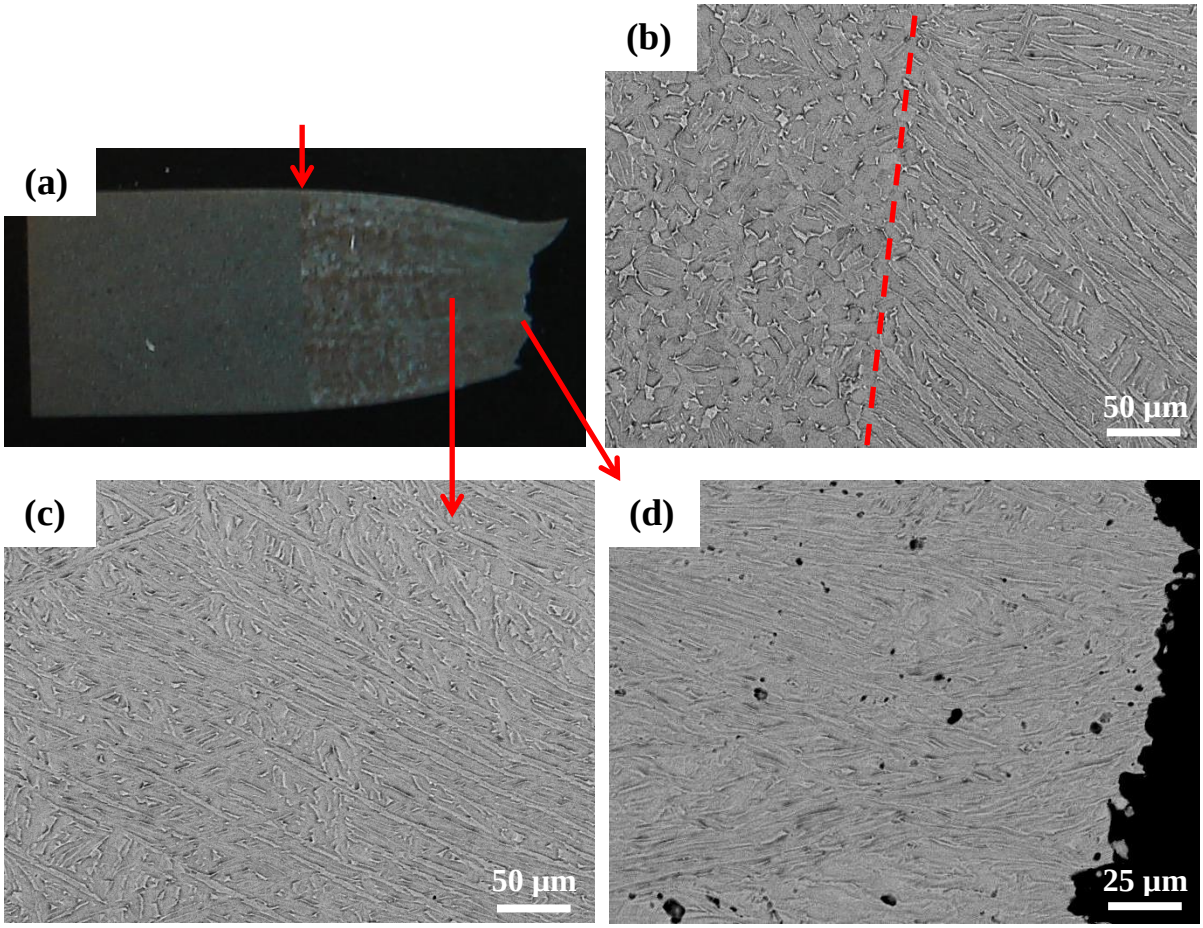

Fig. 9 (a) Photograph showing a longitudinal section of a sample after tensile testing, suggesting that failure happened on the side of shell; SEM micrographs showing (b) the interface (indicated by the arrow) between the HIPed powder and the tooling remaining intact after tensile testing; (c) lamellar structure deformed towards necking; (d) cavity developed near fracture surfaces.